

ARTICLE OPEN



Nonreciprocal charge transport in topological superconductor candidate $\text{Bi}_2\text{Te}_3/\text{PdTe}_2$ heterostructure

Makoto Masuko¹, Minoru Kawamura²✉, Ryutarō Yoshimi², Motoaki Hirayama^{1,2}, Yuya Ikeda¹, Ryota Watanabe¹, James Jun He², Denis Maryenko², Atsushi Tsukazaki³, Kei S. Takahashi², Masashi Kawasaki^{1,2}, Naoto Nagaosa^{1,2} and Yoshinori Tokura^{1,2,4}

In a hybrid system of topological insulator (TI)/superconductor (SC), the proximity-induced topological superconductivity is expected to appear at the interface. Here we propose and demonstrate that a TI/SC hybrid $\text{Bi}_2\text{Te}_3/\text{PdTe}_2$ heterostructure serves as a platform for exploring topological superconductivity with various features: all made of tellurium compounds, epitaxial growth, and a small charge transfer interface. In the $\text{Bi}_2\text{Te}_3/\text{PdTe}_2$ heterostructure films, we observe large nonreciprocal charge transport near the superconducting transition temperature under a transverse in-plane magnetic field. The observation indicates the interplay between the topological surface state and superconductivity, suggesting that the $\text{Bi}_2\text{Te}_3/\text{PdTe}_2$ heterostructure is a candidate for a topological superconductor. Also observed is an unexpected sign reversal of the nonreciprocal coefficient when the in-plane magnetic field is slightly tilted toward the out-of-plane direction. The analysis reveals that the sign reversal occurs with the change of dominant vortex type, that is, the change from spontaneous vortices to external-field induced ones.

npj Quantum Materials (2022)7:104; <https://doi.org/10.1038/s41535-022-00514-x>

INTRODUCTION

Realization and utilization of topological superconductors hosting Majorana fermions have recently been attracting enormous interest¹. One promising way to realize topological superconductivity is to fabricate a hybrid system of topological insulator (TI)/s-wave superconductor (SC), where topological superconductivity of the spinless chiral p -wave can be induced by the proximity effect at the spin-momentum locked surface of the TI². So far, the TI/SC hybrid systems have been explored in a wide range of materials, mostly classified into two groups according to their structures. One is a system where a thin film of TI is grown on a single crystal of an SC^{3–5}. Spectroscopic measurements such as angle-resolved photoemission spectroscopy⁵ or scanning tunneling microscopy/spectroscopy^{3,4} have been carried out to characterize the system while fabrication of elaborate devices utilizing the Majorana fermions would be difficult in this type of system. The other is a system where elemental SC, such as Nb or Al, is deposited on a thin film of TI^{6–9}. Selective area growth or etching technique enables the fabrication of devices such as Josephson junctions. Using these devices, non-trivial transport properties of proximity-induced topological superconductivity have been demonstrated. To realize innovative topological SC devices with chiral Majorana fermion modes, it is necessary to tune the chemical potential into the bulk bandgap of TI. However, tuning is difficult in these systems due to a large amount of charge transfer between elemental SC and TI. Thus, it is highly desired to establish a materials platform of TI/SC hybrid compatible with the device fabrication and the chemical-potential tuning¹⁰.

Nonreciprocal charge transport, or so-called diode effect, has been investigated as a sensitive probe to the inversion symmetry breaking. The nonreciprocal charge transport originally studied in non-centrosymmetric crystals or interfaces under magnetic fields¹¹ has been recently extended to the two-dimensional (2D) superconductors without inversion symmetry^{12–14}. In the TI/SC

hybrid systems, the interplay between the inversion-symmetry-broken surface state of the TI and the superconductor is expected to give rise to the nonreciprocal charge transport^{14,15}. A recent experimental study on a TI/SC hybrid system $\text{Bi}_2\text{Te}_3/\text{NbSe}_2$ has revealed the effect of the external in-plane magnetic field on the normal state Fermi surface by scanning tunneling microscopy/spectroscopy¹⁶.

In this paper, we propose and demonstrate that $\text{Bi}_2\text{Te}_3/\text{PdTe}_2$ heterostructure serves as a platform for exploring topological superconductivity. We chose Bi_2Te_3 and PdTe_2 as TI and SC, respectively, and fabricated a $\text{Bi}_2\text{Te}_3/\text{PdTe}_2$ thin-film heterostructure. The $\text{Bi}_2\text{Te}_3/\text{PdTe}_2$ heterostructure is a TI/SC hybrid system all made of epitaxially grown tellurium compounds. The first-principles calculation of the electronic band structure shows a minimal charge transfer through the interface owing to the close electronegativity in the two tellurium compounds. Large nonreciprocal resistance is observed around the superconducting transition temperature under an in-plane magnetic field perpendicular to the current direction, indicating inversion symmetry breaking of the electronic state at the interface. We further observe the sign reversal of the nonreciprocal coefficient when the magnetic field is tilted to the out-of-plane direction. The sign reversal is associated with the crossover in the type of the dominant vortex from the spontaneous to the field-induced one.

RESULTS

Electronic structure in $\text{Bi}_2\text{Te}_3/\text{PdTe}_2$ heterostructure

A superconductor 1T- PdTe_2 with a superconducting transition temperature $T_c = 1.7$ K is a member of transition-metal dichalcogenides¹⁷. PdTe_2 shares many common features in the crystal structure with Bi_2Te_3 ; both have layered van der Waals structures consisting of Te-terminated triangular lattices with comparable lattice constants (Fig. 1a). The chemical and structural similarities

¹Department of Applied Physics and Quantum Phase Electronics Center (QPEC), University of Tokyo, Tokyo 113-8656, Japan. ²RIKEN Center for Emergent Matter Science (CEMS), Wako 351-0198, Japan. ³Institute for Materials Research, Tohoku University, Sendai 980-8577, Japan. ⁴Tokyo College, University of Tokyo, Tokyo 113-8656, Japan.

✉email: minoru@riken.jp

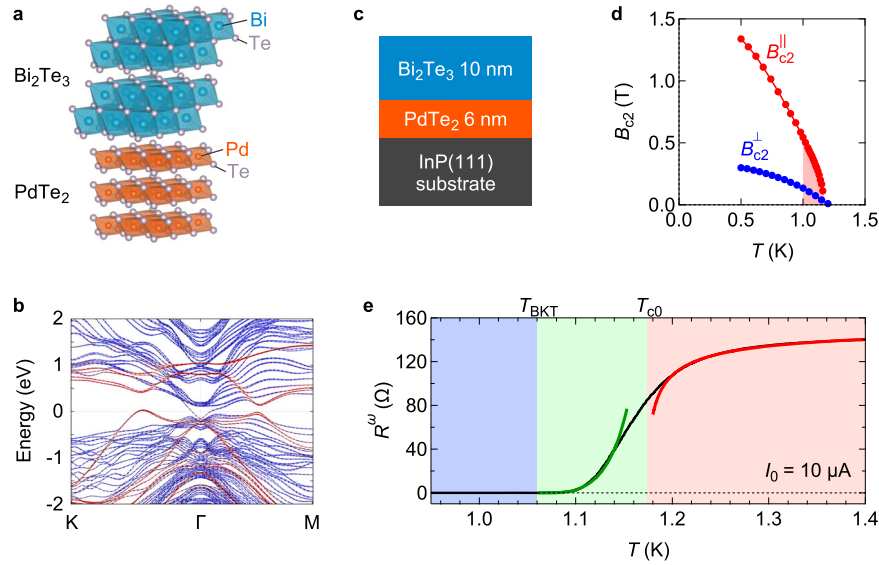


Fig. 1 Electronic structure and superconductivity of Bi₂Te₃/PdTe₂ heterostructure. **a** Crystal structure of Bi₂Te₃ and PdTe₂. **b** Band structure of PdTe₂ (1 layer)/Bi₂Te₃ (6 layers)/PdTe₂ (1 layer). The red and blue lines correspond to the states originating from PdTe₂ and Bi₂Te₃, respectively. **c** Schematic of the thin-film heterostructure. **d** Temperature dependence of in-plane and out-of-plane upper critical fields, B_{c2}^{\parallel} (red) and B_{c2}^{\perp} (blue). Nonreciprocal transport is studied in the red-shaded parameter region. **e** Temperature dependence of R^{ω} measured under $I_0 = 10 \mu\text{A}$. The red curve is the fit by the Aslamazov–Larkin formula, $\Delta G = \frac{e^2}{16\hbar} \frac{T_{c0}}{T - T_{c0}}$, where $\Delta G = (R^{\omega})^{-1} - R_N^{-1}$. The fitting parameters are $T_{c0} = 1.174 \text{ K}$ and $R_N = 153 \Omega$. The green curve is the fit by the Halperin–Nelson formula $R^{\omega} = R_c \exp\left(-2\sqrt{\frac{b(T_{c0}-T)}{T - T_{\text{BKT}}}}\right)$, where $R_c = 457 \Omega$ and $b = 3.50$ are material-dependent fitting parameters, and $T_{\text{BKT}} = 1.060 \text{ K}$ is the BKT transition temperature estimated from the power law of current–voltage characteristics (Supplementary Fig. 5). T_{BKT} and T_{c0} separate the temperature into three regions: zero-resistance (blue), free vortices (green), and paraconductivity (red).

between Bi₂Te₃ and PdTe₂ suggest that they can be an ideal combination to form a TI/SC heterostructure^{18,19}. We fabricated a thin film of Bi₂Te₃/PdTe₂ on an InP(111)A substrate by molecular beam epitaxy (see the “Methods” section). The epitaxial growth of thin films and heterostructures of Bi₂Te₃ and PdTe₂ are confirmed by the X-ray diffraction (see Supplementary Fig. 1 in Supplementary Information), the cross-section transmission electron microscopy (TEM), and energy-dispersive X-ray (EDX) spectroscopy (Supplementary Fig. 2). The heterostructure has a sharp interface and the elemental intermixing at the interface is negligibly small. In a relatively thick film (e.g. 45 nm) of PdTe₂ on InP(111)A substrate, a sharp superconducting transition is observed at 1.7 K, which is consistent with bulk crystals¹⁷ and previously reported thin films²⁰. As the thickness is reduced, e.g. down to 6 nm, T_c becomes low, and the superconducting transition becomes broad (see Supplementary Fig. 3 for the details).

To investigate the electronic state in Bi₂Te₃/PdTe₂ heterostructures, we have performed the first-principles calculations of the electronic band structure (see the “Methods” section for details). Figure 1b shows the band structure for PdTe₂ (1 layer)/Bi₂Te₃ (6 layers)/PdTe₂ (1 layer). Here, the thickness of the TI Bi₂Te₃ layer, 6 layers, is chosen to be thick enough to avoid the formation of a hybridization gap between the top and bottom surface states. Around the Γ point, the topological surface states originating from Bi₂Te₃ are formed. Small carrier pockets from bulk bands indicate the small charge transfer between Bi₂Te₃ and PdTe₂. The common use of tellurium with close electronegativity results in reduced charge transfer, in contrast to the case of, e.g. Nb/Bi₂Te₃ with large charge transfer, making the Bi₂Te₃/PdTe₂ heterostructure an ideal platform of TI/SC hybrid. Most importantly, the Fermi level of the heterostructure appears to cross the interface Dirac dispersion, strongly suggesting the formation of topological superconductivity.

Two-dimensional superconductivity in Bi₂Te₃/PdTe₂

We first investigate the superconducting transport properties in the heterostructure film of Bi₂Te₃ (10 nm)/PdTe₂ (6 nm) (Fig. 1c) in a Hall-bar-shaped sample (see the “Methods” section). Figure 1e shows the temperature T dependence of the first harmonic (Ohmic) resistance R^{ω} around the superconducting transition. Due to the thin PdTe₂ layer (6 nm), it is expected to realize a two-dimensional superconducting state. In fact, the R^{ω} - T curve can be described with the Aslamazov–Larkin formula on a high-temperature side²¹ and with the Halperin–Nelson formula on a low-temperature side²². Red curve in Fig. 1e is the fit by the Aslamazov–Larkin formula of the paraconductivity²¹, $\Delta G = \frac{e^2}{16\hbar} \frac{T_{c0}}{T - T_{c0}}$, where $\Delta G = (R^{\omega})^{-1} - R_N^{-1}$ is the excess conductance, R_N is the normal state resistance, and T_{c0} is the mean-field critical temperature. The fitting parameters are $R_N = 153 \Omega$ and $T_{c0} = 1.174 \text{ K}$. Note that R_N is dominated by the 6-nm-thick PdTe₂ layer and that the resistance of the 10-nm-thick Bi₂Te₃ layer is approximately 3 times larger than that (see Supplementary Fig. 4). Green curve in Fig. 1e is the fit by the Halperin–Nelson formula of two-dimensional superconducting transition²¹, $R^{\omega} = R_c \exp\left(-2\sqrt{\frac{b(T_{c0}-T)}{T - T_{\text{BKT}}}}\right)$, where $R_c = 457 \Omega$ and $b = 3.50$ are materials parameters and $T_{\text{BKT}} = 1.060 \text{ K}$ is the Beresinskii–Kosterlitz–Thouless (BKT) transition temperature estimated from the current–voltage characteristics (see Supplementary Fig. 5). The temperature dependence of resistivity and the current–voltage characteristics verify the two-dimensionality of the superconductivity with the BKT transition^{23,24}. Because of the nature of 2D superconductivity, free vortices and antivortices are spontaneously formed below T_{c0} . In the temperature regime $T_{\text{BKT}} < T < T_{c0}$ represented by a green area in Fig. 1e, the resistance is generated by the current-induced motion of the vortices. Formation of vortex–antivortex pairs results in the zero-

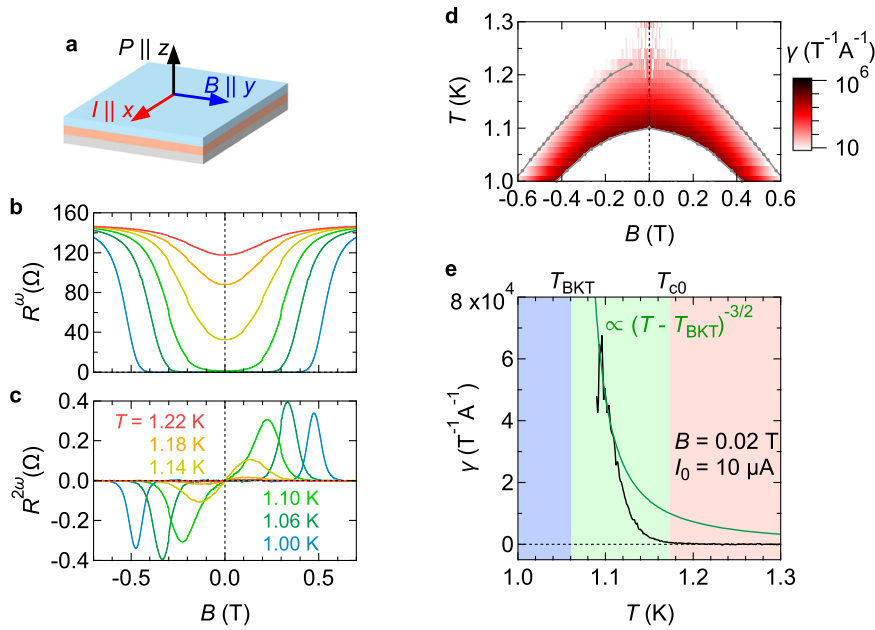


Fig. 2 Nonreciprocal transport under in-plane magnetic field. **a** Schematic illustration of the measurement configuration. **b, c** Magnetic field dependence of R^ω (**b**) and $R^{2\omega}$ (**c**) at various temperatures. **d** Color plot of γ as a function of magnetic field and temperature. γ is derived using the relation $R^{2\omega} = \frac{1}{\sqrt{2}} \gamma R^\omega B l_0$. Gray lines, respectively, show the curves with equal resistance of $R^\omega = 1$ and 120Ω . **e** Temperature dependence of nonreciprocal coefficient γ at $B = 0.02 \text{ T}$ and $l_0 = 10 \mu\text{A}$ (black). The theoretical curve with the formula $\gamma = \gamma_0 (T - T_{\text{BKT}})^{-3/2}$ (green) is also plotted, where $\gamma_0 = 380 \text{ T}^{-1} \text{ A}^{-1} \text{ K}^{1.5}$.

resistance state below T_{BKT} . In Fig. 1d, the temperature dependence of the in-plane and out-of-plane upper critical fields, B_{c2}^{\parallel} and B_{c2}^{\perp} are shown, which are defined here by the midpoints of the normal state resistance. B_{c2}^{\parallel} is larger than B_{c2}^{\perp} , which is typical of 2D superconductors^{23,24}.

Nonreciprocal transport under in-plane magnetic field

Next, we investigated the nonreciprocal charge transport near the superconducting transition. Figure 2a schematically illustrates the experimental configuration for the nonreciprocal transport measurement. We applied current I along the x -axis and magnetic field B along the y -axis (in-plane). In $\text{Bi}_2\text{Te}_3/\text{PdTe}_2$, the mirror symmetry with respect to the xy -plane is broken at the interface (polar axis $\mathbf{P} \parallel \mathbf{z}$, where \mathbf{z} is a unit vector normal to the film plane). The resistance R in a polar system under a magnetic field \mathbf{B} is phenomenologically described¹¹ as $R = R_0 [1 + \gamma (\mathbf{B} \times \mathbf{z}) \cdot \mathbf{I}]$, where R_0 is the resistance at zero magnetic fields and γ is the nonreciprocal coefficient. Therefore, the nonreciprocal transport (the second term) is expected to emerge in the configuration shown in Fig. 2a. The voltage–current characteristic is represented by $V = R_0 I + \gamma R_0 B I^2$ including the I -linear (Ohmic) and I -square (nonreciprocal) terms. Under the application of an AC current $I(t) = \sqrt{2} I_0 \sin(\omega t)$, in addition to the first-harmonic voltage $V^\omega = \sqrt{2} R_0 I_0 \sin(\omega t)$, the second-harmonic voltage $V^{2\omega} = -\gamma R_0 B I_0^2 \cos(2\omega t)$ appears reflecting the I -square term. From the measured V^ω and $V^{2\omega}$, we obtained the first harmonic (Ohmic) resistance $R^\omega(B)$ as well as the nonreciprocal resistance $R^{2\omega}(B) = \frac{1}{\sqrt{2}} \gamma R_0 B I_0$. Considering the symmetry of the system, we symmetrized (anti-symmetrized) R^ω ($R^{2\omega}$) with respect to B .

Figures 2b, c respectively, show the magnetic field dependence of R^ω and $R^{2\omega}$ at various temperatures measured in the configuration in Fig. 2a. As the temperature decreases below 1.22 K, the nonreciprocal resistance $R^{2\omega}$ appears under the in-plane magnetic fields. The peak position of $R^{2\omega}$ shifts to the large magnetic fields as the temperature is lowered. The emergence of non-zero $R^{2\omega}$ in Fig. 2c indicates the realization of fluctuating

Table 1. Comparison of γ' in 2D superconductors.

Material	$T_{c,\text{mid}}$ (K)	γ' ($\text{T}^{-1} \text{ A}^{-1} \text{ m}$)	Reference
$\text{Bi}_2\text{Te}_3/\text{PdTe}_2$	1.16	6.8	Present study
$\text{MoS}_2\text{-EDLT}$	8.8	2.4×10^{-2}	12
$\text{Bi}_2\text{Te}_3/\text{FeTe}$	10	6.5×10^{-3}	14
NbSe_2	6.5	2.19×10^{-1}	25

superconductivity without inversion symmetry. We confirmed that $R^{2\omega}$ almost vanishes for $B \parallel I$ as expected from the symmetry (see Supplementary Fig. 6). $R^{2\omega}$ in Fig. 2c is enhanced in the magnetic field range where R^ω transits between 0 and the normal resistance. This trend can be clearly seen in Fig. 2d, the color plot of nonreciprocal coefficient $\gamma = \frac{\sqrt{2} R^{2\omega}}{R_0 B I_0}$ in the magnetic field–temperature plane. In the region between the two gray curves of $R^\omega = 120$ and 1Ω , which respectively, correspond to the normal states and the zero-resistance states, γ is remarkably enhanced. Above the upper gray curve, where superconductivity is broken, γ is significantly suppressed. Note that γ is difficult to evaluate for $R^\omega < 1 \Omega$ due to the smallness of both R^ω and $R^{2\omega}$. The largest value of γ in this plane is $6.8 \times 10^4 \text{ T}^{-1} \text{ A}^{-1}$ at $B = 0.02 \text{ T}$ and $T = 1.10 \text{ K}$. Table 1 compares the observed nonreciprocal coefficient in the present study with those reported in the previous studies on noncentrosymmetric 2D superconductors^{12,14,25}. In the table, γ' is the normalized value of the nonreciprocal coefficient by the Hall bar width w ($\gamma' = \gamma w$, $w = 100 \mu\text{m}$ in the present study). Large values of γ' tend to appear in materials with small T_c . In the case of metals/semiconductors, the nonreciprocal coefficient is known to be inversely proportional to the Fermi energy¹¹. The observed trend can be understood by substituting the Fermi energy with the superconducting gap.

As a check, we have also explored the nonreciprocal transport in ZnTe (10 nm)/ PdTe_2 (6 nm), where a trivial insulator ZnTe is used instead of a topological insulator Bi_2Te_3 . The observed

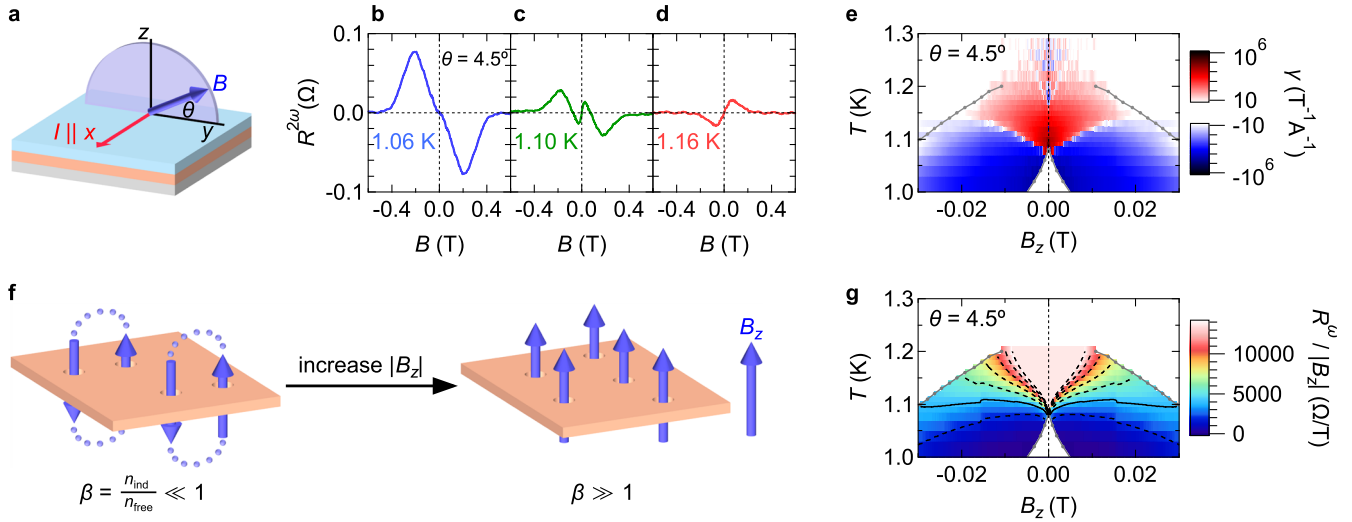


Fig. 3 Impact of out-of-plane magnetic field on the nonreciprocal transport. **a** Schematic of the measurement configuration. θ is defined as the tilting angle of magnetic field B from the in-plane y -axis. **b–d** Magnetic field dependence of $R^{2\omega}$ at 1.06, 1.10, and 1.16 K for $\theta = 4.5^\circ$. **e** Color plot of γ in the B_z – T plane at $\theta = 4.5^\circ$ ($B_z = B \sin \theta$). **f** Schematics of the free-vortices dominant state (left, $\beta \ll 1$) and induced-vortices dominant one (right, $\beta \gg 1$) with $\beta \equiv n_{\text{ind}}/n_{\text{free}}$. As $|B_z|$ increases, the crossover from the free-vortices dominant state to the induced-vortices dominant one is expected to occur. **g** Color plot of $R^\omega/|B_z|$ in the B_z – T plane at $\theta = 4.5^\circ$. Contour lines for $R^\omega/|B_z| = 2000, 4000, \dots, 14000 \Omega\text{T}^{-1}$ are plotted by black dotted lines. The solid line corresponds to $R^\omega/|B_z| = 4000 \Omega\text{T}^{-1}$.

nonreciprocal signal in ZnTe/PdTe₂ is much smaller than Bi₂Te₃/PdTe₂ (see Supplementary Fig. 6), indicating that the proximity effect of SC to the surface state of TI is necessary for the emergence of the large nonreciprocal response.

Figure 2e shows the temperature dependence of γ (black curve) at $B = 0.02$ T obtained from the temperature dependence of R^ω and $R^{2\omega}$. γ increases steeply with decreasing temperature below T_{co} . In $T_{\text{BKT}} < T < T_{\text{co}}$, the resistance R is generated by the motion of spontaneously formed free vortices²², and it can be written as $R = \frac{\phi_0^2}{\eta} n_{\text{free}}$. Here, $\phi_0 = h/2e$ is the magnetic flux quantum, η is the friction coefficient of vortex motion, and n_{free} is the density of free vortices. The temperature dependence of free vortex density, $n_{\text{free}} \propto \exp\left(-2\sqrt{\frac{b(T_{\text{co}}-T)}{T-T_{\text{BKT}}}}\right)$ (valid for $\frac{T-T_{\text{BKT}}}{T_{\text{co}}-T_{\text{BKT}}} \ll 1$), is the origin of the characteristic exponential temperature dependence of R in the BKT transition²². A recent theory considering a topological surface state with a superconducting gap shows that external current renormalizes the superfluid density¹⁵. As a result, T_{BKT} becomes current dependent, $T_{\text{BKT}} = T_{\text{BKT}}^0(1 + \Lambda B_y I)$, with Λ a material parameter. Accordingly, this renormalizes n_{free} as $n_{\text{free}}(I) = n_{\text{free}}(0) \left[1 - \frac{T_{\text{BKT}}^0 \sqrt{b(T_{\text{co}} - T_{\text{BKT}}^0)}}{(T - T_{\text{BKT}}^0)^{\frac{3}{2}}} \Lambda B_y I\right]$ to the first order of $\Lambda B_y I$. Because the resistance R is proportional to n_{free} , the second term gives rise to the nonreciprocal resistance. Hence, γ is proportional to $(T - T_{\text{BKT}}^0)^{-\frac{3}{2}}$ at temperatures near T_{BKT}^0 and thus expected to diverge at T_{BKT}^0 . The observed temperature dependence of γ is compared with the formula $\gamma = \gamma_0 (T - T_{\text{BKT}}^0)^{-\frac{3}{2}}$ with $\gamma_0 = 380 \text{ T}^{-1} \text{ A}^{-1} \text{ K}^{1.5}$ as shown in Fig. 2e. The increasing trend in γ with decreasing T roughly agrees with the theoretical curve. The consistency supports that the observed nonreciprocal transport can be understood in terms of the current-induced modulation of the superfluidity density in the superconducting proximity-coupled TI surface state.

Nonreciprocal transport under tilted magnetic field

Finally, we discuss the nonreciprocal transport when the magnetic field is slightly tilted toward the out-of-plane (z) direction, as illustrated in Fig. 3a. Figure 3b–d depict representative magnetic

field dependence of $R^{2\omega}$ at 1.06, 1.10, and 1.16 K for $\theta = 4.5^\circ$ (see the “Methods” section for the measurement of θ). Similarly to the case of an in-plane magnetic field ($\theta = 0^\circ$), $R^{2\omega}$ appears, but the sign of $R^{2\omega}$ under $B > 0$ varies depending on temperature and magnetic field strength. This makes a stark contrast to the result for $\theta = 0^\circ$ where $R^{2\omega}$ under $B > 0$ is always positive. To demonstrate the sign reversal of the nonreciprocal response more clearly, we show in Fig. 3e the color contour plot of γ in the B_z – T plane, where $B_z = B \sin \theta$ is the out-of-plane component of the magnetic field. At low $|B_z|$ and high temperature, positive γ is observed as in the case of the genuine in-plane magnetic field (Fig. 2d). On the other hand, at high $|B_z|$ and low temperature, negative γ shows up. It is noteworthy that, when the magnetic field is tilted toward the $-z$ direction ($\theta < 0$), a similar sign-reversal of γ is observed (see Supplementary Fig. 7 for the full data).

To obtain further insight into the sign reversal of γ , we consider a model involving spontaneous free vortices and vortices induced by B_z (Fig. 3f). When $|B_z|$ is weak enough, free vortices and antivortices with the density n_{free} are thermally excited (Fig. 3f left). On the other hand, when $|B_z|$ is strong enough but still smaller than B_{c2}^\perp , vortices induced by B_z become dominant (Fig. 3f right), and their density is expressed by $n_{\text{ind}} = |B_z|/\phi_0$. We suggest in our model that the crossover between dominant vortex types is related to the sign-reversal of γ , which is observed only under the tilted magnetic field. Therefore, we introduce the ratio $\beta = n_{\text{ind}}/n_{\text{free}}$. To experimentally estimate the value of β , we assume that the Ohmic resistance R^ω is proportional to the total number of vortices: $R^\omega = \frac{\phi_0^2}{\eta} (n_{\text{free}} + n_{\text{ind}})$.

This relationship can be rewritten as $\frac{R^\omega}{|B_z|} = \frac{\phi_0}{\eta} \left(1 + \frac{1}{\beta}\right)$ to give a one-to-one correspondence between β and the experimentally measured value of $R^\omega/|B_z|$. Thus, using the experimental data, we produce in Fig. 3g the contour plot of $R^\omega/|B_z|$ in the B_z – T plane for $\theta = 4.5^\circ$. The increase in $|B_z|$ or decrease in T leads to the reduction in $R^\omega/|B_z|$, reflecting the increase in the population of the induced vortices and hence in β . By comparing the color plots of γ in Fig. 3e and $R^\omega/|B_z|$ in Fig. 3g, one can find that the boundary between regions of $\gamma > 0$ and $\gamma < 0$ coincides qualitatively with the contour line of $R^\omega/|B_z| = \text{const.}$ (dotted and solid black lines). Such correspondence between the two contour plots indicates that the sign of γ is determined by $R^\omega/|B_z|$, or in other words, by β , supporting the validity of our model. γ is positive on the free-

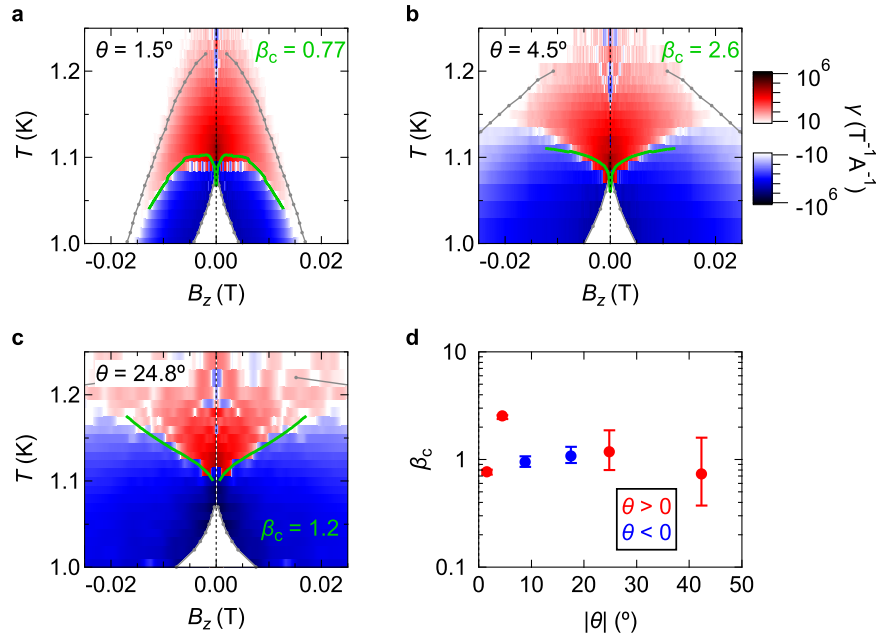


Fig. 4 Sign reversal of the nonreciprocal coefficient under various magnetic field tilted angles. **a–c** Color plots of γ with the contour lines of $\frac{\beta_c}{|\beta_z|} = \left(1 + \frac{1}{\beta_c}\right) \frac{\phi_0}{\eta}$ (green) in the B_z – T plane for $\theta = 1.5^\circ$, 4.5° , and 24.8° . The value β_c is estimated such that the curve $\frac{\beta_c}{|\beta_z|} = \left(1 + \frac{1}{\beta_c}\right) \frac{\phi_0}{\eta}$ gives the best fitting to the boundary between the regions with $\gamma > 0$ (red) and $\gamma < 0$ (blue). **d** β_c as a function of the tilt angle θ . The data for $\theta > 0$ ($\theta < 0$) are represented by red (blue).

vortices dominant side with small β and changes its sign on the induced-vortices dominant side with large β .

Figures 4a–c show the color plots of γ in the B_z – T plane for $\theta = 1.5^\circ$, 4.5° , and 24.8° . For each θ , we have estimated the critical ratio β_c such that the curve $\frac{\beta_c}{|\beta_z|} = \frac{\phi_0}{\eta} \left(1 + \frac{1}{\beta_c}\right)$ gives the best fitting to the boundary between the regions with $\gamma > 0$ and $\gamma < 0$. The fitting results are shown by green curves. In all cases, the boundary is well fit by the curves with comparable values of β_c close to unity, as shown in Fig. 4d. This analysis indicates that β determines the sign of γ regardless of θ . In this fitting analysis, we used a constant value of $\eta \sim 0.68 \text{ nm}^2 \text{ T}^2 \Omega^{-1}$ at $T = T_{\text{BKT}}$ (see Supplementary Note 1 for the estimation of η).

DISCUSSION

The above analysis has shown that both spontaneous and field-induced vortices give rise to nonreciprocal transport in $\text{Bi}_2\text{Te}_3/\text{PdTe}_2$, while the sign of γ is defined by the dominant vortex type. Besides our system, the nonreciprocal charge transport originating from vortex dynamics has been studied in various 2D superconductors^{12–14,25}, which can be classified into two groups according to the orientation of the polar axis \mathbf{P} : out-of-plane polar ones (polar axis $\mathbf{P} \parallel z$ -axis) and in-plane polar ones ($\mathbf{P} \parallel xy$ -plane). Reflecting the orientation of \mathbf{P} , the direction of the magnetic field necessary for the emergence of nonreciprocity is different between these two groups, leading to the difference in the type of vortices. In the out-of-plane polar systems, which are represented by $\text{Bi}_2\text{Te}_3/\text{FeTe}$ ¹⁴ or gate-induced superconductivity in SrTiO_3 ¹³, the nonreciprocal transport governed by the motion of spontaneous free vortices has been investigated under in-plane magnetic fields. In contrast, in the systems with the in-plane breaking of inversion symmetry, as exemplified by gate-induced superconductivity in MoS_2 ¹², the nonreciprocity due to the dynamics of vortices induced by out-of-plane magnetic fields has been verified. The present $\text{Bi}_2\text{Te}_3/\text{PdTe}_2$ system with the out-of-plane polarity shows a different symmetry from the in-plane

polarity case for MoS_2 . Nevertheless, the motion of induced vortices governs the nonreciprocal charge transport with negative γ ; this is an unconventional situation of the polar 2D superconductors or possibly of the interface topological superconductors. In this case, the coexistence of B_y and B_z is essential; B_z induces vortices, while the breaking of both time-reversal symmetry and mirror symmetry by B_y is a prerequisite for the emergence of nonreciprocity.

The sign change in γ depending on the type of vortices indicates that the different microscopic mechanisms of nonreciprocal response are at work. The nonreciprocal transport with the positive γ in the free-vortices dominant situation has been elucidated by the current-induced renormalization of superfluid density, which results in the current direction dependence of n_{free} ¹⁵. On the other hand, when the number of field-induced vortices is fixed by B_z , the asymmetry in the motion of vortices should be the main mechanism of nonreciprocal resistivity. One of the most likely candidates is the ratchet-type potential for the vortex motion, although the sign of γ depends on the details of the potential in the material²⁶. Further theoretical and experimental investigation is required to fully reveal the origin of negative γ .

We also note that the superconducting diode effect²⁷, which is the non-reciprocity in the superconducting critical current, has recently been reported in a multilayer superconductor system. Several theoretical studies predict the non-reciprocity in the superconducting critical current in the presence of Rashba-type spin–orbit interaction^{28–30}, while these theories are not directly applicable to the BKT regime of the present study.

In summary, we have fabricated a $\text{Bi}_2\text{Te}_3/\text{PdTe}_2$ thin-film heterostructure as a TI/SC hybrid system and investigated the nonreciprocal charge transport arising from the motion of vortices. Under an in-plane magnetic field, large nonreciprocal signals have been observed near the superconducting transition temperature. Moreover, we have observed the sign reversal of γ by tilting the magnetic field toward the out-of-plane direction. The

observed sign reversal of γ has been consistently explained by the scenario that γ is positive (negative) when the motion of spontaneous vortices (field-induced vortices) generates resistance. The appearance of nonreciprocal charge transport is clear evidence for the inversion symmetry broken superconductivity in the $\text{Bi}_2\text{Te}_3/\text{PdTe}_2$ heterostructure, suggesting that the superconducting proximity effect on the TI surface state is effective. Our study suggests that $\text{Bi}_2\text{Te}_3/\text{PdTe}_2$ can be a good materials platform to explore proximity-induced topological superconductivity. Fabrication of $\text{Bi}_2\text{Te}_3/\text{PdTe}_2$ -based thin-film devices will lead to the direct detection of topological superconductivity or Majorana fermions.

METHODS

Thin-film growth and device fabrication

We grew the heterostructure film by molecular beam epitaxy (MBE). The base pressure of the MBE growth chamber was on the order of 10^{-7} Pa. Thin film samples were grown on semi-insulating $\text{InP}(111)\text{A}$ substrates. Molecular beam fluxes of Bi and Te were supplied from standard Knudsen cells and that of Pd was from a special Knudsen cell customized for high-temperature operation. The beam equivalent pressures of Pd, Bi, and Te were set at 3.3×10^{-7} , 5.0×10^{-6} , and 1.0×10^{-4} Pa, respectively. The substrate temperature was set at 340°C throughout the growth. The beam fluxes of Pd and Bi were turned on/off by controlling the shutters. The growth rates were 0.25 and 0.29 nm/min for PdTe_2 and Bi_2Te_3 , respectively. The substrate was rotated during the growth to improve the homogeneity of the film. After the growth, the substrate heater was turned off and the substrate was cooled to room temperature and taken out of the growth chamber. Then, the grown film was transferred to the chamber of atomic layer deposition and covered with a 3-nm-thick AlO_x deposited at room temperature for the passivation.

The samples were characterized by X-ray diffraction (XRD) with $\text{Cu K}\alpha 1$ radiation. After the thin-film growth, Hall bar devices were defined using ultraviolet photolithography and Ar ion milling. Both the width w and the distance between the voltage probes were 100 μm . The electrodes Au (25 nm)/Ti (5 nm) were formed by electron beam deposition.

Transport measurements

Transport measurement was conducted using a ^3He cooling system of a physical property measurement system (PPMS, Quantum Design). In the nonreciprocal transport measurement, we used copper plates bent at different angles, and the sample was mounted on a copper plate fixed on a sample puck. The tilt angle of magnetic field θ was estimated from the Hall effect at 300 K. We applied AC current using an AC current source (Keithley, model 6221) and measured the first and second harmonic voltages using digital lock-in amplifiers (Stanford Research Systems, model SR830). The measurement current and frequency were 10 μA (root mean square) and 37 Hz, respectively.

First-principles calculation for the electronic structure of $\text{Bi}_2\text{Te}_3/\text{PdTe}_2$ heterostructure

We employed the Vienna Ab initio Simulation Package (VASP)³¹ for the ab initio calculation based on the density functional theory (DFT). We used the projector augmented wave (PAW)³² potential sets recommended by VASP and set the kinetic-energy cutoff to 350 eV. In the calculations of the lattice optimization and the electronic band structure, we employed the generalized-gradient approximation (GGA) with the Perdew–Burke–Ernzerhof parameterization for solid (PBEsol)³³ without the spin–orbit interaction and the GGA of the Perdew–Burke–Ernzerhof (PBE)³⁴ with the spin–orbit interaction, respectively. We employed the $6 \times 6 \times 1$ \mathbf{k}

mesh for the lattice optimization and the $8 \times 8 \times 1$ \mathbf{k} mesh for the calculation of the electronic band structure. We used the in-plane lattice constant of Bi_2Te_3 as that of the interface system. We have confirmed that there is no qualitative difference in the band structure when using the lattice constant of PdTe_2 (Supplementary Fig. 8).

DATA AVAILABILITY

The data that support the findings of this study are available from the corresponding author upon reasonable request.

Received: 22 May 2022; Accepted: 14 October 2022;

Published online: 30 October 2022

REFERENCES

- Sato, M. & Ando, Y. Topological superconductors: a review. *Rep. Prog. Phys.* **80**, 076501 (2017).
- Fu, L. & Kane, C. L. Superconducting proximity effect and Majorana fermions at the surface of a topological insulator. *Phys. Rev. Lett.* **100**, 096407 (2008).
- Xu, J. P. et al. Experimental detection of a Majorana mode in the core of a magnetic vortex inside a topological insulator–superconductor $\text{Bi}_2\text{Te}_3/\text{NbSe}_2$ heterostructure. *Phys. Rev. Lett.* **114**, 017001 (2015).
- Zhao, H. et al. Superconducting proximity effect in a topological insulator using $\text{Fe}(\text{Te},\text{Se})$. *Phys. Rev. B* **97**, 224504 (2018).
- Wang, E. et al. Fully gapped topological surface states in Bi_2Se_3 films induced by a d-wave high-temperature superconductor. *Nat. Phys.* **9**, 621–625 (2013).
- Wiedenmann, J. et al. 4π -periodic Josephson supercurrent in HgTe-based topological Josephson junctions. *Nat. Commun.* **7**, 10303 (2016).
- Schüffelgen, P. et al. Selective area growth and stencil lithography for in situ fabricated quantum devices. *Nat. Nanotechnol.* **14**, 825–831 (2019).
- Kayyalha, M. et al. Absence of evidence for chiral Majorana modes in quantum anomalous Hall-superconductor devices. *Science* **367**, 64–67 (2020).
- Williams, J. R. et al. Unconventional Josephson effect in hybrid superconductor–topological insulator devices. *Phys. Rev. Lett.* **109**, 056803 (2012).
- Qi, X. L., Hughes, T. L. & Zhang, S. C. Chiral topological superconductor from the quantum Hall state. *Phys. Rev. B* **82**, 184516 (2010).
- Tokura, Y. & Nagaosa, N. Nonreciprocal responses from non-centrosymmetric quantum materials. *Nat. Commun.* **9**, 3740 (2018).
- Wakatsuki, R. et al. Nonreciprocal charge transport in noncentrosymmetric superconductors. *Sci. Adv.* **3**, e1602390 (2017).
- Itahashi, Y. et al. Nonreciprocal transport in gate-induced polar superconductor SrTiO_3 . *Sci. Adv.* **6**, eaay9120 (2020).
- Yasuda, K. et al. Nonreciprocal charge transport at topological insulator/superconductor interface. *Nat. Commun.* **10**, 2734 (2019).
- Hoshino, S., Wakatsuki, R., Hamamoto, K. & Nagaosa, N. Nonreciprocal charge transport in two-dimensional noncentrosymmetric superconductors. *Phys. Rev. B* **98**, 054510 (2018).
- Zhu, Z. et al. *Science* **374**, 1381–1385 (2021).
- Teknowijoyo, S. et al. Nodeless superconductivity in the type-II Dirac semimetal PdTe_2 : London penetration depth and pairing-symmetry analysis. *Phys. Rev. B* **98**, 024508 (2018).
- Xue, H. Y. et al. Molecular beam epitaxy of superconducting PdTe_2 films on topological insulator Bi_2Te_3 . *Sci. China Phys. Mech. Astron.* **62**, 76801 (2019).
- Bai, M. et al. Novel self-epitaxy for inducing superconductivity in the topological insulator $(\text{Bi}_{1-x}\text{Sb}_x)_2\text{Te}_3$. *Phys. Rev. Mater.* **4**, 094801 (2020).
- Liu, C. et al. Two-dimensional superconductivity and topological states in PdTe_2 thin films. *Phys. Rev. Mater.* **2**, 094001 (2018).
- Aslamasov, L. G. & Larkin, A. I. The influence of fluctuation pairing of electrons on the conductivity of normal metal. *Phys. Lett. A* **26**, 238–239 (1968).
- Halperin, B. I. & Nelson, D. R. Resistive transition in superconducting films. *J. Low Temp. Phys.* **36**, 599–616 (1979).
- Saito, Y., Nojima, T. & Iwasa, Y. Highly crystalline 2D superconductors. *Nat. Rev. Mater.* **2**, 16094 (2016).
- Tinkham, M. *Introduction to Superconductivity* 2nd edn (Dover, New York, 2004).
- Zhang, E. et al. Nonreciprocal superconducting NbSe_2 antenna. *Nat. Commun.* **11**, 5634 (2020).
- Hamamoto, K., Park, T., Ishizuka, H. & Nagaosa, N. Scaling theory of a quantum ratchet. *Phys. Rev. B* **99**, 064307 (2019).
- Ando, F. et al. Observation of superconducting diode effect. *Nature* **584**, 373–376 (2020).

28. Daido, A., Ikeda, Y. & Yanase, Y. Intrinsic superconducting diode effect. *Phys. Rev. Lett.* **128**, 037001 (2022).
29. Yuan, N. F. Q. & Fu, L. Supercurrent diode effect and finite momentum superconductors. *Proc. Natl Acad. Sci. USA* **119**, e2119548119 (2022).
30. He, J. J., Tanaka, Y. & Nagaosa, N. A phenomenological theory of superconductor diodes. *N. J. Phys.* **24**, 053014 (2022).
31. Kresse, G. & Furthmüller, J. Efficient iterative schemes for ab initio total-energy calculations using a plane-wave basis set. *Phys. Rev. B* **54**, 11169 (1996).
32. Blöchl, P. E. Projector augmented-wave method. *Phys. Rev. B* **50**, 17953 (1994).
33. Perdew, J. P. et al. Restoring the density-gradient expansion for exchange in solids and surfaces. *Phys. Rev. Lett.* **100**, 136406 (2008).
34. Perdew, J. P., Burke, K. & Ernzerhof, M. Generalized gradient approximation made simple. *Phys. Rev. Lett.* **77**, 3865 (1996).

ACKNOWLEDGEMENTS

We thank Y. Iwasa for the fruitful discussions. M.M. is supported by the Japan Society for the Promotion of Science (JSPS) through a research fellowship for young scientists (No. 19J22547). This research was supported by the Japan Society for the Promotion of Science through JSPS/MEXT Grant-in-Aid for Scientific Research (Nos. 18H01155, 18H03676, 20K14390), and JST CREST (Nos. JPMJCR16F1, JPMJCR1874).

AUTHOR CONTRIBUTIONS

Y.T. conceived the project. M.M., R.Y. and Y.I. grew the thin films with the help of A.T., K.S.T. and M.Kawasaki. M.M. and Y.I. performed the measurement with help from M. Kawamura, R.Y., R.W. and D.M. M.H. performed the band calculation. M.M., M. Kawamura, R.Y., M.H., J.J.H., N.N. and Y.T. analyzed and interpreted the data. M.M., M. Kawamura, and Y.T. jointly wrote the manuscript with contributions from all authors.

COMPETING INTERESTS

The authors declare no competing interests.

ADDITIONAL INFORMATION

Supplementary information The online version contains supplementary material available at <https://doi.org/10.1038/s41535-022-00514-x>.

Correspondence and requests for materials should be addressed to Minoru Kawamura.

Reprints and permission information is available at <http://www.nature.com/reprints>

Publisher's note Springer Nature remains neutral with regard to jurisdictional claims in published maps and institutional affiliations.



Open Access This article is licensed under a Creative Commons Attribution 4.0 International License, which permits use, sharing, adaptation, distribution and reproduction in any medium or format, as long as you give appropriate credit to the original author(s) and the source, provide a link to the Creative Commons license, and indicate if changes were made. The images or other third party material in this article are included in the article's Creative Commons license, unless indicated otherwise in a credit line to the material. If material is not included in the article's Creative Commons license and your intended use is not permitted by statutory regulation or exceeds the permitted use, you will need to obtain permission directly from the copyright holder. To view a copy of this license, visit <http://creativecommons.org/licenses/by/4.0/>.

© The Author(s) 2022